# Ice-proximal sea-ice reconstruction in Powell Basin, Antarctica since the Last Interglacial

**Wee Wei Khoo et al.**

## S1: Age model

The age model of marine sediment core PS118_63-1 was first established using a comparative analysis between the XRF-Ti record with the EDML $\delta^{18}O$ record (Supplementary Fig. S1). Furthermore, the MIS 5/6 boundary is identified by the biostratigraphic marker *Rouxia leventerae* (ca. 130 ka BP; Zielinski et al., 2002). Since <1% relative abundance of *Rouxia leventerae* was found at core depth 6.19 m (0.6%), we estimated the last occurrence of *Rouxia leventerae* to be around 6.2 m. Planktic foraminifera were also selected for AMS $^{14}C$-dating (Supplementary Table S1) using the Mini Carbon Dating System at the Alfred Wegener Institute (AWI), Bremerhaven, Germany. The $^{14}C$ ages were calibrated to calendar ages using the PaleoDataView software (v0.9.5.25; Heaton et al., 2020; Langner and Mulitza, 2019).

Additionally, to further refine the age model, we considered age control tie points identified in records from a nearby marine core U1537 (MS, XRF-Fe and Opal) and the EDML ice core (ssNa+). See Supplementary Fig. S2 for the tie points identified in the respective records of marine core PS118_63-1 with marine core U1537 and EDML ice core. The tuning of these cores with marine core PS118_63-1 was conducted using the QAnalyseries software (v1.5.1; Kotov and Pälike, 2018). A summary of the tie points used for the establishment of the age model of marine core PS118_63-1 is provided in Supplementary Table S2. To account for age uncertainty, we imposed an age error of ±1 kyr for all the tuning tie points, with the exception of four tie points from U1537-MS. We adopted the age errors from the age model of U1537 for these four tie points instead (refer also to Supplementary Table 2 of Weber et al., 2022). Lastly, the Bayesian age-depth modeling was established using Bacon v2.5.8 (Blaauw and Christen, 2011) on RStudio v2022.07.02.

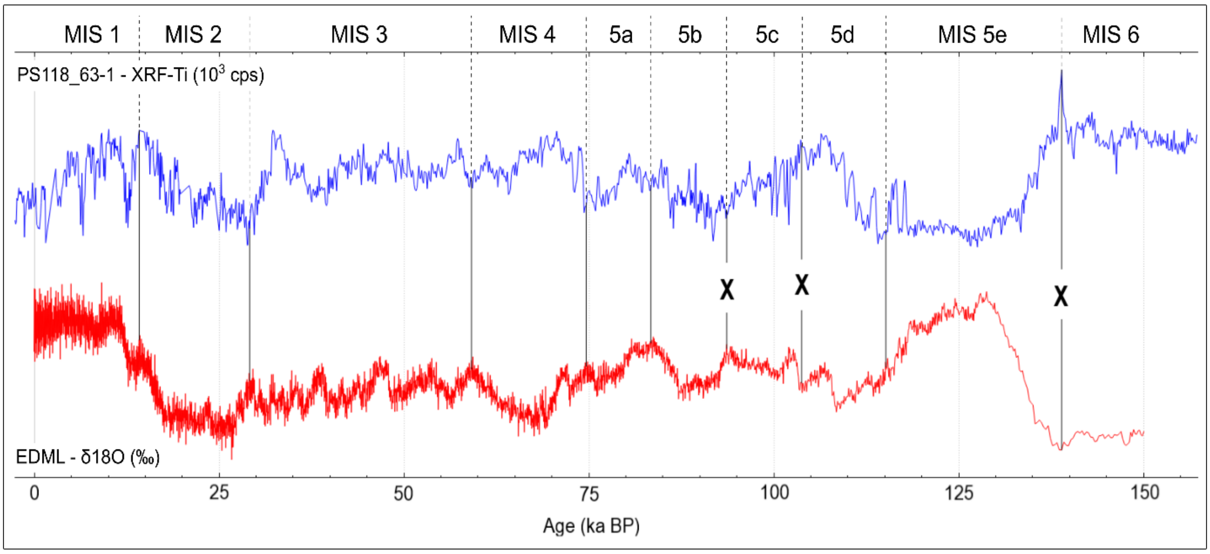


**Supplementary Figure S1**. Age-depth profile of marine sediment core PS118_63-1 against that of the EDML $\delta^{18}O$ record. Black crosses indicate tie points that were not chosen for use in the age model after careful comparison between each age control tie points. Age intervals for MIS 1 - 4 and 6 are in accordance to Lisiecki and Raymo (2005) and MIS 5 substages are referenced to Bianchi and Gersonde (2002).

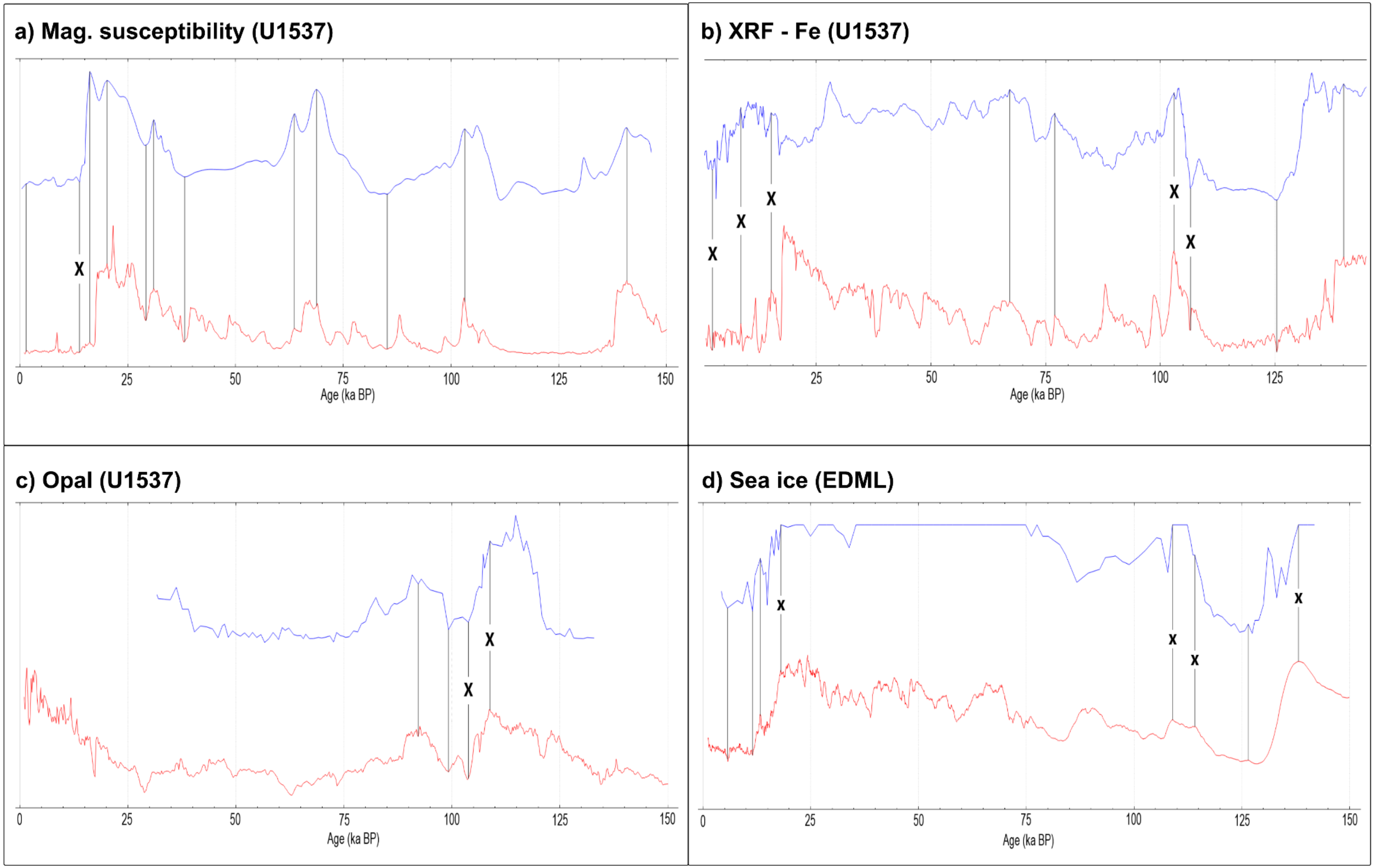


**Supplementary Figure S2**. Plots of age control tie points identified in records a) magnetic susceptibility, b) XRF – Fe and c) opal records of marine core U1537 (red) against marine core PS118_63-1 (blue), and d) EDML ssNa+ record (red) against that of the $PIPSO_{25}$ record from marine core PS118_63-1 (blue). Black crosses indicate tie points that were not selected for inclusion in the age model after careful comparison between the respective records.

**Supplementary Table S1**. Radiocarbon dates taken from marine sediment core PS118_63-1.

| Sample Name | AWI Nr. | Material | $F^{14}C$ | ± (abs) | $^{14}C$ age (kyrs) | $\pm^{14}C$ age (kyrs) | Cal age (ka BP) | ± cal age (kyrs) |
|---|---|---|---|---|---|---|---|---|
| PS118_63-1_ 163-165cm | 9742.1.1 | *N. pachyderma* | 0.1259 | 0.0025 | 16.647 | 0.158 | 17.603 | 0.935 |
| PS118_63-1_ 179-181cm | 9743.1.1 | *N. pachyderma* | 0.0845 | 0.0023 | 19.850 | 0.221 | 21.422 | 0.862 |

**Supplementary Table S2**: Tie points used for age-depth model for marine sediment core PS118_63-1.

| S/N | MIS | Depth (m) | Age (ka BP) | ± Age (kyrs) | Tie point |
|---|---|---|---|---|---|
| 1 | 1 | 0.076 | 1.2 | 1 | U1537-MS |
| 2 | 1 | 0.125 | 5.772 | 1 | EDML-ssNa+ |
| 3 | 1 | 0.625 | 10.675 | 1 | EDML-ssNa+ |
| 4 | 1 | 0.925 | 13.352 | 1 | EDML-ssNa+ |
| 5 | 1 | 1 | 14 | 1 | EDML-$\delta^{18}O$ |
| 6 | 2 | 1.516 | 16.2 | 1 | U1537-MS |
| 7 | 2 | 1.64 | 17.603 | 0.935^ | $^{14}C$-dating |
| 8 | 2 | 1.706 | 20 | 1 | U1537-MS |
| 9 | 2 | 1.8 | 21.422 | 0.862^ | $^{14}C$-dating |
| 10 | 3 | 2 | 29 | 1 | EDML-$\delta^{18}O$ |
| 11 | 3 | 2.018 | 29.21 | 0.78* | U1537-MS |
| 12 | 3 | 2.098 | 31.2 | 1 | U1537-MS |
| 13 | 3 | 2.548 | 38 | 1 | U1537-MS |
| 14 | 4 | 3.1 | 57 | 1 | EDML-$\delta^{18}O$ |
| 15 | 4 | 3.228 | 63.64 | 2.28* | U1537-MS |
| 16 | 4 | 3.46 | 67.2 | 1 | U1537-Fe |
| 17 | 4 | 3.478 | 68.8 | 2.1* | U1537-MS |
| 18 | 5a | 3.6 | 74 | 1 | EDML-$\delta^{18}O$ |
| 19 | 5a | 3.84 | 76.8 | 1 | U1537-Fe |
| 20 | 5b | 3.9 | 83 | 1 | EDML-$\delta^{18}O$ |
| 21 | 5b | 4.028 | 85 | 1 | U1537-MS |
| 22 | 5b | 4.33 | 92 | 1 | U1537-Opal |
| 23 | 5c | 4.83 | 99.2 | 1 | U1537-Opal |
| 24 | 5d | 4.868 | 103.17 | 1.71* | U1537-MS |
| 25 | 5e | 5.25 | 114 | 1 | EDML-$\delta^{18}O$ |
| 26 | 5e | 5.68 | 125.2 | 1 | U1537-Fe |
| 27 | 5e | 5.83 | 126.336 | 1 | EDML-ssNa+ |
| 28 | 6 | 6.2 | 130 | 1 | *R. leventarae* |
| 29 | 6 | 6.56 | 139.8 | 1 | U1537-Fe |
| 30 | 6 | 6.588 | 140.6 | 1 | U1537-MS |

^Age error taken from calibrated age uncertainty (refer to Supplementary Table S1)
*Age error adopted from age model for marine core U1537 (refer to Supplementary Table 2 of Weber et al., 2022)

## S2: $^{230}$Th-excess constant-rate-of-supply model

To estimate the $^{230}$Th-excess constant-rate-of-supply (CRS) age model for PS118_63-1, a total of 54 freeze-dried, grounded and homogenized sediment samples were selected (at specific depth intervals) for the determination of uranium (U) and thorium (Th) isotopes ($^{230}$Th, $^{232}$Th, $^{238}$U and $^{234}$U). The samples were first digested in a pressure-assisted microwave digestion system (CEM MarsXpress; 24 samples per batch). Following which, 15 mL of the digested solution underwent a separation and purification process via the seaFAST automatic column separation system, using TRU resin. Each Th/U fraction was then analyzed via sector-field inductively coupled plasma mass spectrometry (SF-ICP-MS Element2). U-isotopes were measured in low resolution using a cyclonic spray chamber while Th-isotopes were measured with an Apex IR desolvation device for increasing ion yield, and in a custom-made resolution of R=2000 for increasing abundance sensitivity. The methods employed in the determination of $^{230}$Th-excess and subsequent CRS-dating for PS118_63-1 are described in Geibert et al. (2019), with the calculation of the CRS age following a method by Appleby and Oldfield (1978).

The robustness of the age model for PS118_63-1 determined using 30 tie points (Supplementary Table S2) is supported by the strong correlation between the tie points-derived age model and estimations via the $^{230}$Th-excess CRS-dating approach (Supplementary Fig. S3). The deviations are to be expected considering possible changes in focusing and the limited $^{230}$Th-inventory considered in this core.

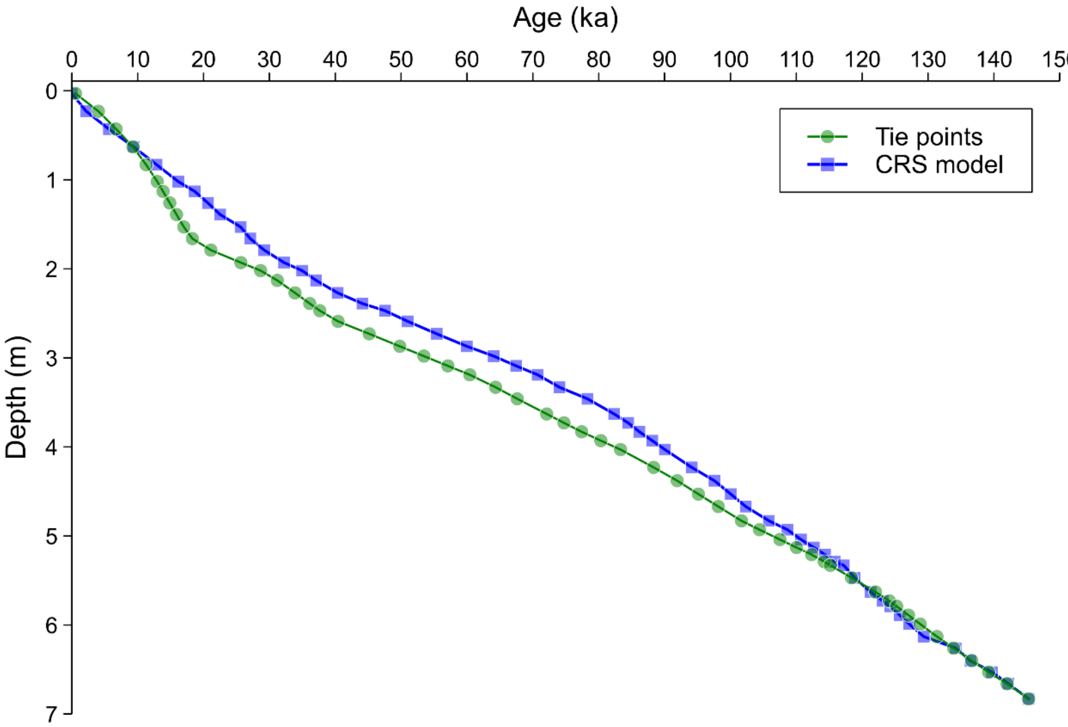


**Supplementary Figure S3.** Comparison of age-depth profile of PS118_63-1 established based on tie points and $^{230}$Th-excess CRS model.

## S3: Numerical model and climate simulations

### 3.1 Community Earth System Models

The Community Earth System Models (COSMOS) have been successfully applied for the study of both colder and warmer than present climates – during, and beyond, the Cenozoic, both at orbital and tectonic time scales. In many cases, the COSMOS have helped to improve our understanding of inferences from the geologic record. They have provided a dynamical framework of relevant processes in the climate system that may mechanistically explain reconstructed climate patterns. Examples for this work include simulations of the climates of the Cretaceous (Klages et al., 2020), of the Miocene (Knorr and Lohmann, 2014; Stein et al., 2016), of the Pliocene (Stepanek et al., 2020), of the Penultimate Glacial (Stein et al., 2017), of the LIG (Gierz et al., 2017; Pfeiffer and Lohmann, 2016; Stein et al., 2017), of the LGM (Zhang et al., 2013), and of the Holocene (Guagnin et al., 2016). Furthermore, the model has been employed towards a large number of process studies. Among these are the works by Knorr et al. (2021) on glacial termination, the study by Kaboth-Bahr et al. (2021) on the delay of Northern Hemisphere glaciation by Mediterranean heat injection into the North Atlantic Ocean, the publication by Zhang et al. (2021) on the impact of astronomical forcing on Pleistocene millennial climate variability, and the investigation by Lohmann et al. (2022) on the potential contribution of increased vertical mixing towards reduced meridional temperature gradients in warm climates of the Pliocene and Miocene.

### 3.2 Modelled climate states

The climate states *piControl*, *mh6k*, *lgm21k*, *lig125k*, and *pgm140k* are derived from equilibrium climate simulations, where we analyze the climate state at the end of a spin up. In these cases, the COSMOS have been instantaneously exposed to reconstructions of greenhouse gases and of orbital forcing, and to paleogeography, if applicable. An exception to this methodology is the LIG climate state at 128 ka BP, derived from simulation *lig128k*. This simulation stems from the computation of a transient evolution of LIG climate from 130 ka BP to 115 ka BP, where the COSMOS have been employed with time-varying greenhouse gas concentrations and orbital forcing applying an acceleration of a factor of 10. The initial ocean state at 130 ka BP has been created to mirror conditions that are representative for the penultimate deglaciation, Termination II (TII; 140 – 130 ka BP). This ocean state has been created based on a weak hosing (0.05 Sv) under perpetual 130 ka BP forcing. To derive the climate conditions at 128 ka BP, we average the transient model climate state over the 100 model years that refer to the period from 128.5 ka BP to 127.5 ka BP. Details of the model setups of the various simulations are provided in Supplementary Table S3.

**Supplementary Table S1**. Boundary conditions and model forcings for climate simulations. We present: forcing values of eccentricity of the Earth's orbit (ecc), obliquity of the Earth's rotation axis (obld), longitude of the perihelion of the Earth's orbit (lonp); atmospheric concentrations of greenhouse gas species carbon dioxide ($CO_2$), methane, ($CH_4$), nitruous oxide ($N_2O$); where applicable, references (ref) to employed paleogeography, orbital forcing, atmospheric greenhouse gas forcing, and to a study that previously described the simulation are provided.

| **Simulation** | **Orbital forcing** | | | | **Greenhouse gas forcing** | | | | **Paleography** | | **Previously published by** | |
|---|---|---|---|---|---|---|---|---|---|---|---|---|
| | **ecc** | **obld (°)** | **Lonp (°)** | **ref** | **$CO_2$ (ppm)** | **$CH_4$ (ppb)** | **$N_2O$ (ppb)** | **ref** | **reconstruction** | **ref** | **ref** | **name in ref** |
| piControl | 0.016724 | 23.4468 | 282.157 | Berger (1978) | 280 | 760 | 270 | Crucifix et al. (2005) | — | — | Wei and Lohmann (2012) | CTL |
| mh6k | 0.018682 | 24.1048 | 180.918 | Berger (1978) | 280 | 650 | 270 | Crucifix et al. (2005) (as PMIP3 6ka) | — | — | Wei and Lohmann (2012) | H6K |
| lgm21k | 0.018994 | 22.949 | 114.42 | Braconnot and Kageyama (2015) and references therein | 185 | 350 | 200 | PMIP3 21ka Braconnot and Kageyama (2015) and references therein | PMIP3 21ka | Braconnot and Kageyama (2015) and references therein | Zhang et al. (2013) | LGMW |
| lig125k | 0.040013 | 23.798 | 127.14 | PMIP3 125ka Lunt et al. (2013) | 275.938 | 640.417 | 263.084 | PMIP3 125ka Lunt et al. (2013) | as piControl | — | this study | — |
| lig128k | 0.039017 | 24.131 | 79.65 | PMIP3 128ka Lunt et al. (2013) | 275 | 709 | 512 | 128ka Lunt et al. (2013) | as piControl | — | this study | — |
| pgm140k | 0.032796 | 23.4138 | 253.244 | Berger et al. (1978) | 185 | 350 | 200 | as lgm21k | as lgm21k | as lgm21k | this study | — |

## S4: Productivity signals

The concentration of total isoprenoid glycerol dialkyl glycerol tetraether lipids (isoGDGTs) and hydroxylated (OH)-isoGDGTs, synthetized from marine archaea (Schouten et al., 2013), varies between 1.36 – 358.32 µg/g OC and 0.01 – 105.71 µg/g OC, respectively. The concentration of total branched GDGTs (brGDGTs), mainly derived from terrestrial bacteria or eukaryotes in soils and peats (Hopmans et al., 2004), ranges between 0.11 and 7.34 µg/g OC. Lastly, the concentration of phytosterols fluctuates between 0 – 54.28 µg/g OC (Brassicasterol) and 0 – 8.51 µg/g OC (Dinosterol). The brassicasterol and opal ($bSiO_2$) profiles, often used as diatom productivity indicators, exhibit contrasting trends, especially between 140 – 110 ka BP. This discrepancy likely arises from the limited presence of brassicasterol-producing diatoms in the area, further affected by preferential growth conditions and preservation effects. As a result, the brassicasterol-producing diatoms signal is consistently attenuated within the overall opal signal (Badejo et al., 2017; Cavagna et al., 2013).

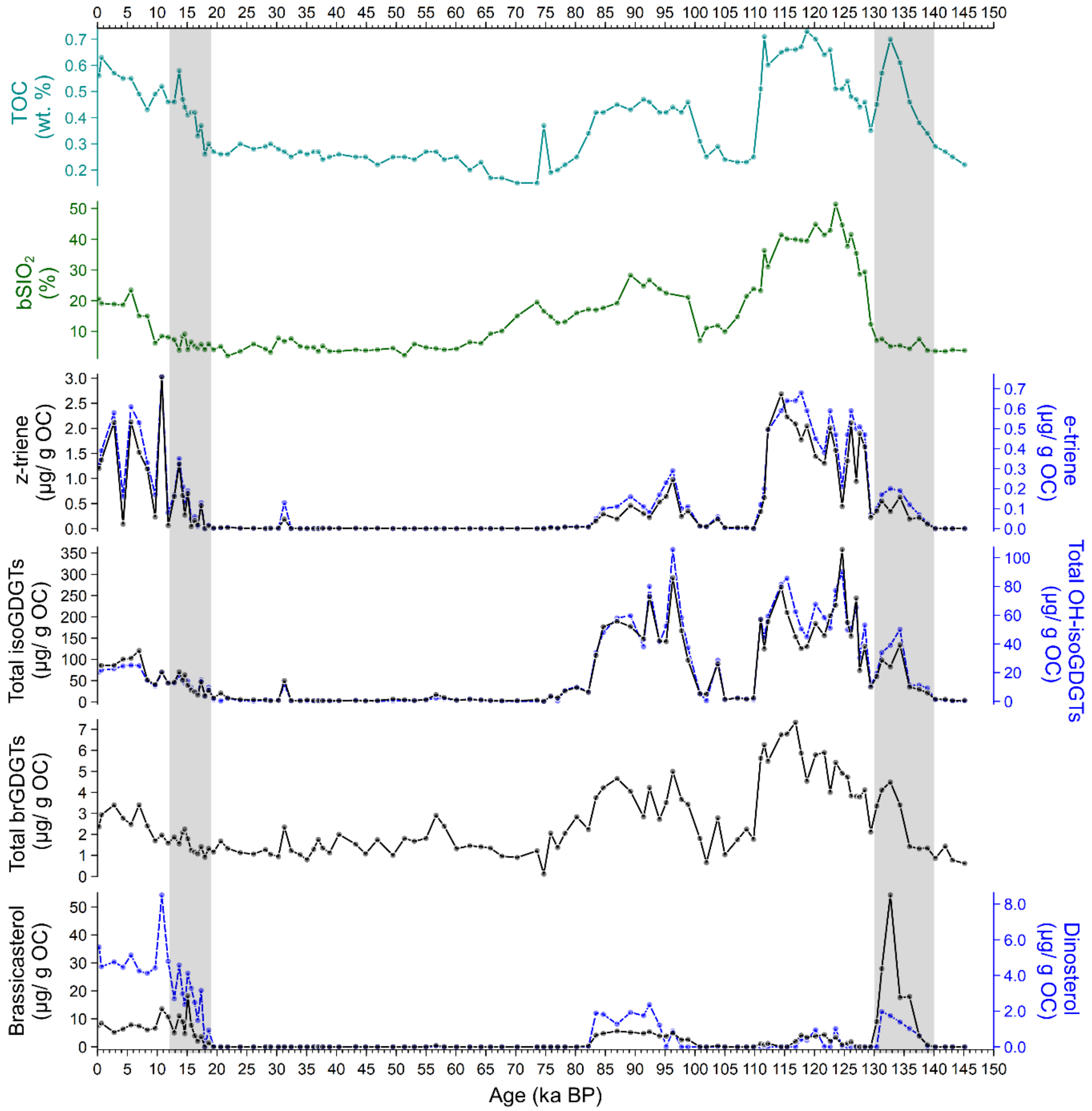


**Supplementary Figure S4**. Plots of organic matter signals from core PS118_63-1. From top to bottom: TOC, biogenic opal, HBI-based phytoplankton, total isoprenoid-GDGTs, total branched-GDGTs and phytosterols. Shaded intervals indicate Termination 1 and Termination II, respectively.

## S5: $TEX_{86}^{L}$-derived subsurface ocean temperature and GDGT-related indices

The $TEX_{86}^{L}$-derived subsurface ocean temperature (OT) shows a temperature range between -2.58 and 0.98°C at the core site. However, a review of the GDGT-related indices provides strong evidence of factors that result in biasness in our $TEX_{86}^{L}$-based temperature reconstruction, especially during MIS 2 – 4, 5d and 6 (Supplementary Fig. S5). For example, a GDGT-[2]/[3] ratio greater than five indicates contribution from deep-dwelling archaea (>1000 water depth), which are regulated by processes different than that of their surface water counterparts (Kim et al., 2015; Taylor et al., 2013). A higher abundance of isoGDGT-0 relative to crenarchaeol (%GDGT-0 value > 67%) also suggests a methanogenic source for the isoGDGT-0 (Inglis et al., 2015). Lastly, values of ΔRI and BIT indices that are higher than 0.3, imply inputs from potential nonthermal influences and/or terrestrial origin, respectively (Fietz et al., 2016; Park, 2019; Weijers et al., 2006; Zhang et al., 2016).

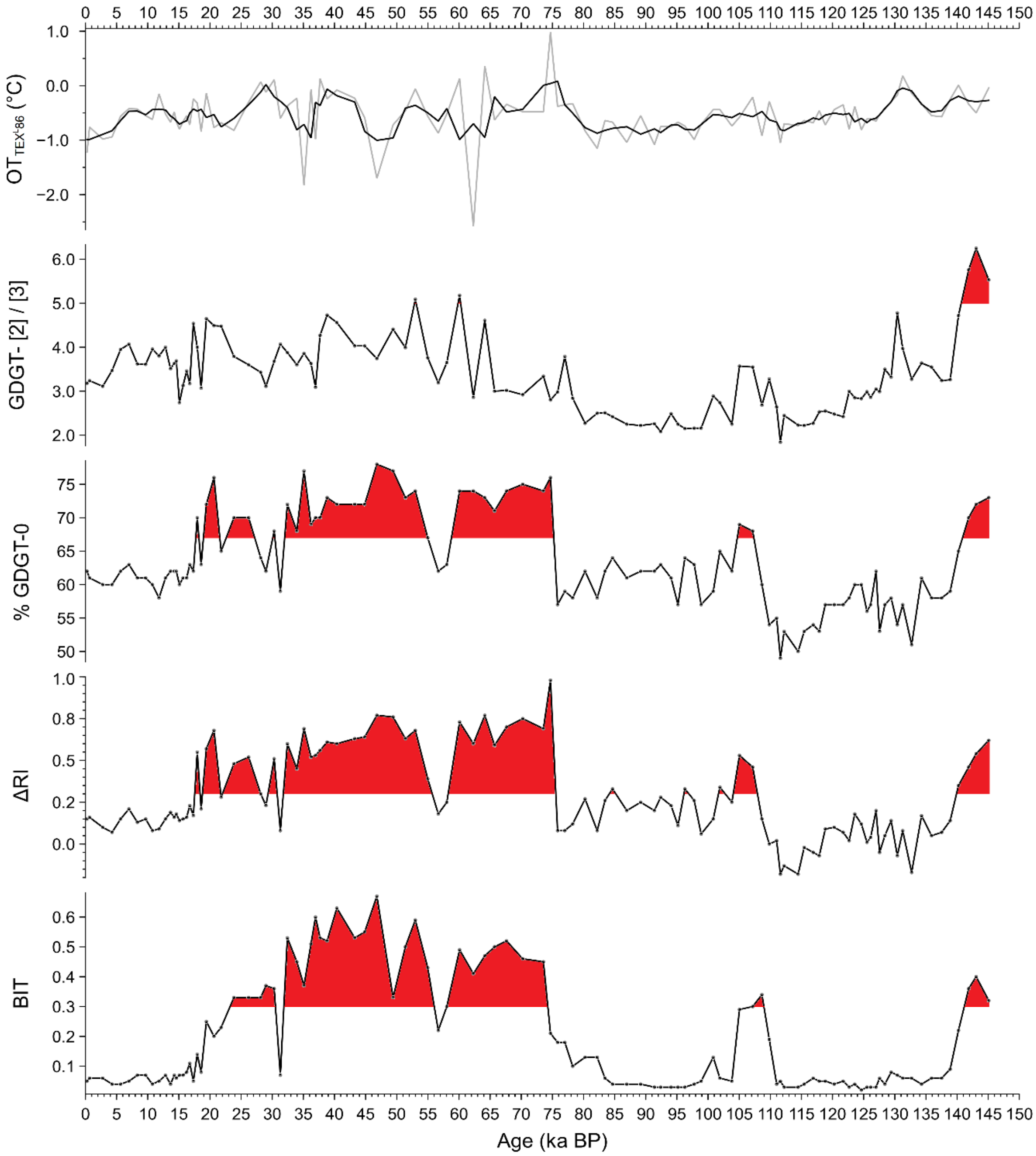


**Supplementary Figure S5.** Records of $TEX^{L}_{86}$ ocean temperature and respective GDGT-related indices: GDGT [2]/[3], %GDGT-0, delta ring index and BIT for core PS118_63-1. Intervals with strong non-thermal influences are highlighted in red on the various index curves: GDGT [2/3] > 5.0, %GDGT-0 > 67%, ΔRI and BIT > 0.3.

## References


Appleby, P. G. and Oldfield, F.: The calculation of lead-210 dates assuming a constant rate of supply of unsupported 210Pb to the sediment, Catena, 5, 1-8, 1978.

Badejo, A. O., Seo, I., Kim, W., Hyeong, K., and Ju, S.-J.: Effect of eolian Fe-supply change on the phytoplankton productivity and community in central equatorial Pacific Ocean during the Pleistocene: A lipid biomarker approach, Organic Geochemistry, 112, 170-176, https://doi.org/10.1016/j.orggeochem.2017.07.010, 2017.

Berger, A.: Long-Term Variations of Daily Insolation and Quaternary Climatic Changes, Journal of Atmospheric Sciences, 35, 2362-2367, https://doi.org/10.1175/1520-0469(1978)035<2362:LTVODI>2.0.CO;2, 1978.

Bianchi, C. and Gersonde, R.: The Southern Ocean surface between Marine Isotope Stages 6 and 5d: Shape and timing of climate changes, Palaeogeography, Palaeoclimatology, Palaeoecology, 187, 151-177, https://doi.org/10.1016/S0031-0182(02)00516-3, 2002.

Blaauw, M. and Christen, J. A.: Flexible paleoclimate age-depth models using an autoregressive gamma process, Bayesian Analysis, 6, 457-474, 418, 2011.

Braconnot, P. and Kageyama, M.: Shortwave forcing and feedbacks in Last Glacial Maximum and Mid-Holocene PMIP3 simulations, Philosophical Transactions of the Royal Society A: Mathematical, Physical and Engineering Sciences, 373, 20140424, doi:10.1098/rsta.2014.0424, 2015.

Cavagna, A. J., Dehairs, F., Bouillon, S., Woule-Ebongué, V., Planchon, F., Delille, B., and Bouloubassi, I.: Water column distribution and carbon isotopic signal of cholesterol, brassicasterol and particulate organic carbon in the Atlantic sector of the Southern Ocean, Biogeosciences, 10, 2787-2801, 10.5194/bg-10-2787-2013, 2013.

Crucifix, M., Braconnot, P., Harrison, S. P., and Otto-Bliesner, B.: Second phase of paleoclimate modelling intercomparison project, Eos, Transactions American Geophysical Union, 86, 264-264, https://doi.org/10.1029/2005EO280003, 2005.

Fietz, S., Ho, S. L., Huguet, C., Rosell-Melé, A., and Martínez-García, A.: Appraising GDGT-based seawater temperature indices in the Southern Ocean, Organic Geochemistry, 102, 93-105, https://doi.org/10.1016/j.orggeochem.2016.10.003, 2016.

Geibert, W., Stimac, I., Rutgers Van Der Loeff, M., and Kuhn, G.: Dating Deep-Sea Sediments With 230Th Excess Using a Constant Rate of Supply Model, Paleoceanography and Paleoclimatology, 34, 1895-1912, https://doi.org/10.1029/2019PA003663, 2019.

Gierz, P., Werner, M., and Lohmann, G.: Simulating climate and stable water isotopes during the Last Interglacial using a coupled climate-isotope model, Journal of Advances in Modeling Earth Systems, 9, 2027-2045, https://doi.org/10.1002/2017MS001056, 2017.

Guagnin, M., Jennings, R., Eager, H., Parton, A., Stimpson, C., Stepanek, C., Pfeiffer, M., Groucutt, H. S., Drake, N. A., Alsharekh, A., and Petraglia, M. D.: Rock art imagery as a proxy for Holocene environmental change: A view from Shuwaymis, NW Saudi Arabia, The Holocene, 26, 1822-1834, 10.1177/0959683616645949, 2016.

Heaton, T. J., Köhler, P., Butzin, M., Bard, E., Reimer, R. W., Austin, W. E., Ramsey, C. B., Grootes, P. M., Hughen, K. A., and Kromer, B.: Marine20—the marine radiocarbon age calibration curve (0–55,000 cal BP), Radiocarbon, 62, 779-820, 2020.

Hopmans, E. C., Weijers, J. W. H., Schefuß, E., Herfort, L., Sinninghe Damsté, J. S., and Schouten, S.: A novel proxy for terrestrial organic matter in sediments based on branched and isoprenoid tetraether lipids, Earth and Planetary Science Letters, 224, 107-116, https://doi.org/10.1016/j.epsl.2004.05.012, 2004.

Inglis, G. N., Farnsworth, A., Lunt, D., Foster, G. L., Hollis, C. J., Pagani, M., Jardine, P. E., Pearson, P. N., Markwick, P., Galsworthy, A. M. J., Raynham, L., Taylor, K. W. R., and Pancost, R. D.: Descent toward the Icehouse: Eocene sea surface cooling inferred from GDGT distributions, Paleoceanography, 30, 1000-1020, https://doi.org/10.1002/2014PA002723, 2015.

Kaboth-Bahr, S., Bahr, A., Stepanek, C., Catunda, M. C. A., Karas, C., Ziegler, M., García-Gallardo, Á., and Grunert, P.: Mediterranean heat injection to the North Atlantic delayed the intensification of Northern Hemisphere glaciations, Communications Earth & Environment, 2, 158, 10.1038/s43247-021-00232-5, 2021.

Kim, J.-H., Schouten, S., Rodrigo-Gámiz, M., Rampen, S., Marino, G., Huguet, C., Helmke, P., Buscail, R., Hopmans, E. C., Pross, J., Sangiorgi, F., Middelburg, J. B. M., and Sinninghe Damsté, J. S.: Influence of deep-water derived isoprenoid tetraether lipids on the TEX86H paleothermometer in the Mediterranean Sea, Geochimica et Cosmochimica Acta, 150, 125-141, https://doi.org/10.1016/j.gca.2014.11.017, 2015.

Klages, J. P., Salzmann, U., Bickert, T., Hillenbrand, C.-D., Gohl, K., Kuhn, G., Bohaty, S. M., Titschack, J., Müller, J., Frederichs, T., Bauersachs, T., Ehrmann, W., van de Flierdt, T., Pereira, P. S., Larter, R. D., Lohmann, G., Niezgodzki, I., Uenzelmann-Neben, G., Zundel, M., Spiegel, C., Mark, C., Chew, D., Francis, J. E., Nehrke, G., Schwarz, F., Smith, J. A., Freudenthal, T., Esper, O., Pälike, H., Ronge, T. A., Dziadek, R., Afanasyeva, V., Arndt, J. E., Ebermann, B., Gebhardt, C., Hochmuth, K., Küssner, K., Najman, Y., Riefstahl, F., Scheinert, M., and the Science Team of Expedition, P. S.: Temperate rainforests near the South Pole during peak Cretaceous warmth, Nature, 580, 81-86, 10.1038/s41586-020-2148-5, 2020.

Knorr, G. and Lohmann, G.: Climate warming during Antarctic ice sheet expansion at the Middle Miocene transition, Nature Geoscience, 7, 376-381, 10.1038/ngeo2119, 2014.

Knorr, G., Barker, S., Zhang, X., Lohmann, G., Gong, X., Gierz, P., Stepanek, C., and Stap, L. B.: A salty deep ocean as a prerequisite for glacial termination, Nature Geoscience, 14, 930-936, 10.1038/s41561-021-00857-3, 2021.

Kotov, S. and Pälike, H.: QAnalySeries-a cross-platform time series tuning and analysis tool, AGU Fall Meeting Abstracts, PP53D-1230,

Langner, M. and Mulitza, S.: Technical note: PaleoDataView – a software toolbox for the collection, homogenization and visualization of marine proxy data, Clim. Past, 15, 2067-2072, 10.5194/cp-15-2067-2019, 2019.

Lisiecki, L. E. and Raymo, M. E.: A Pliocene-Pleistocene stack of 57 globally distributed benthic δ18O records, Paleoceanography, 20, https://doi.org/10.1029/2004PA001071, 2005.

Lohmann, G., Knorr, G., Hossain, A., and Stepanek, C.: Effects of CO2 and Ocean Mixing on Miocene and Pliocene Temperature Gradients, Paleoceanography and Paleoclimatology, 37, e2020PA003953, https://doi.org/10.1029/2020PA003953, 2022.

Lunt, D. J., Abe-Ouchi, A., Bakker, P., Berger, A., Braconnot, P., Charbit, S., Fischer, N., Herold, N., Jungclaus, J. H., Khon, V. C., Krebs-Kanzow, U., Langebroek, P. M., Lohmann, G., Nisancioglu, K. H., Otto-Bliesner, B. L., Park, W., Pfeiffer, M., Phipps, S. J., Prange, M., Rachmayani, R., Renssen, H., Rosenbloom, N., Schneider, B., Stone, E. J., Takahashi, K., Wei, W., Yin, Q., and Zhang, Z. S.: A multi-model assessment of last interglacial temperatures, Clim. Past, 9, 699-717, 10.5194/cp-9-699-2013, 2013.

Park, E.: Variations in GDGT flux and TEX86 thermometry in three distinct oceanic regimes of the Atlantic Ocean: a sediment trap study, University of Bremen, 2019.

Pfeiffer, M. and Lohmann, G.: Greenland Ice Sheet influence on Last Interglacial climate: global sensitivity studies performed with an atmosphere–ocean general circulation model, Clim. Past, 12, 1313-1338, 10.5194/cp-12-1313-2016, 2016.

Schouten, S., Hopmans, E. C., and Damsté, J. S. S.: The organic geochemistry of glycerol dialkyl glycerol tetraether lipids: A review, Organic geochemistry, 54, 19-61, http://dx.doi.org/10.1016/j.orggeochem.2012.09.006, 2013.

Stein, R., Fahl, K., Gierz, P., Niessen, F., and Lohmann, G.: Arctic Ocean sea ice cover during the penultimate glacial and the last interglacial, Nature Communications, 8, 373, 10.1038/s41467-017-00552-1, 2017.

Stein, R., Fahl, K., Schreck, M., Knorr, G., Niessen, F., Forwick, M., Gebhardt, C., Jensen, L., Kaminski, M., Kopf, A., Matthiessen, J., Jokat, W., and Lohmann, G.: Evidence for ice-free summers in the late Miocene central Arctic Ocean, Nature Communications, 7, 11148, 10.1038/ncomms11148, 2016.

Stepanek, C., Samakinwa, E., Knorr, G., and Lohmann, G.: Contribution of the coupled atmosphere–ocean–sea ice–vegetation model COSMOS to the PlioMIP2, Clim. Past, 16, 2275-2323, 10.5194/cp-16-2275-2020, 2020.

Taylor, K. W. R., Huber, M., Hollis, C. J., Hernandez-Sanchez, M. T., and Pancost, R. D.: Re-evaluating modern and Palaeogene GDGT distributions: Implications for SST reconstructions, Global and Planetary Change, 108, 158-174, https://doi.org/10.1016/j.gloplacha.2013.06.011, 2013.

Weber, M. E., Bailey, I., Hemming, S. R., Martos, Y. M., Reilly, B. T., Ronge, T. A., Brachfeld, S., Williams, T., Raymo, M., Belt, S. T., Smik, L., Vogel, H., Peck, V. L., Armbrecht, L., Cage, A., Cardillo, F. G., Du, Z., Fauth, G., Fogwill, C. J., Garcia, M., Garnsworthy, M., Glüder, A., Guitard, M., Gutjahr, M., Hernández-Almeida, I., Hoem, F. S., Hwang, J.-H., Iizuka, M., Kato, Y., Kenlee, B., Oconnell, S., Pérez, L. F., Seki, O., Stevens, L., Tauxe, L., Tripathi, S., Warnock, J., and Zheng, X.: Antiphased dust deposition and productivity in the Antarctic Zone over 1.5 million years, Nature Communications, 13, 2044, 10.1038/s41467-022-29642-5, 2022.

Wei, W. and Lohmann, G.: Simulated Atlantic Multidecadal Oscillation during the Holocene, Journal of Climate, 25, 6989-7002, https://doi.org/10.1175/JCLI-D-11-00667.1, 2012.

Weijers, J. W. H., Schouten, S., Spaargaren, O. C., and Sinninghe Damsté, J. S.: Occurrence and distribution of tetraether membrane lipids in soils: Implications for the use of the TEX86 proxy and the BIT index, Organic Geochemistry, 37, 1680-1693, https://doi.org/10.1016/j.orggeochem.2006.07.018, 2006.

Zhang, X., Lohmann, G., Knorr, G., and Xu, X.: Different ocean states and transient characteristics in Last Glacial Maximum simulations and implications for deglaciation, Clim. Past, 9, 2319-2333, 10.5194/cp-9-2319-2013, 2013.

Zhang, X., Barker, S., Knorr, G., Lohmann, G., Drysdale, R., Sun, Y., Hodell, D., and Chen, F.: Direct astronomical influence on abrupt climate variability, Nature Geoscience, 14, 819-826, 10.1038/s41561-021-00846-6, 2021.

Zhang, Y. G., Pagani, M., and Wang, Z.: Ring Index: A new strategy to evaluate the integrity of TEX86 paleothermometry, Paleoceanography, 31, 220-232, https://doi.org/10.1002/2015PA002848, 2016.

Zielinski, U., Bianchi, C., Gersonde, R., and Kunz-Pirrung, M.: Last occurrence datums of the diatoms Rouxia leventerae and Rouxia constricta: indicators for marine isotope stages 6 and 8 in Southern Ocean sediments, Marine Micropaleontology, 46, 127-137, https://doi.org/10.1016/S0377-8398(02)00042-7, 2002.